



Research paper

Statics and stability of diagonalless beams of particular kind – preliminary studies

Kinga Saternus¹, Przemysław Saternus², Andrzej Szychowski³

Abstract: Attractive large-scale glazing is currently an architectural trend. However, achieving adequate stiffness for larger glazing spans requires the use of complex cross-sections, generally aluminium sections of considerable height. Members with openwork webs are sometimes used in order to achieve increased load-bearing capacity and stiffness with reduced weight. The disadvantage is that this solution takes up a lot of space inside the building. A recently patented diagonalless member attempts to solve the above-mentioned problems. The member is fully demountable and allows glass units to be installed in the space between the chords. It consists of two chords spaced apart by metal sleeves with bolts passed through them. In this study, preliminary qualitative experimental tests were carried out to determine the behaviour of the member under load and to identify zones sensitive to local deformation. On this basis, numerical models (bar and 3D solid models, including contact interactions) were created and tested. Subsequently, the optimum sleeve spacing was determined, the effect of rotational and translational stiffness reduction at the nodes was investigated, and stress concentration zones and forms of stability loss were identified. A new form of local loss of stability of the chord facewall was identified, the so-called sliding push effect of the chord walls on the sleeve (within the larger openings). This is a completely different type of chord facewall failure from that found in known tubular welded joints. The research programme focused on identifying the phenomena occurring in the new member in order to provide a basis for further, more advanced analyses.

Keywords: diagonalless beam, Vierendeel girder, two-chord built-up member, metal sleeve, metal-glass building envelopes, buckling analysis

¹BEng, MSc, Kielce University of Technology, Faculty of Civil Engineering and Architecture, Al. Tysiąclecia Państwa Polskiego 7, 25-314 Kielce, Poland, e-mail: ksaternus@tu.kielce.pl, ORCID: 0000-0001-8516-5004

²BEng, MSc, Kielce University of Technology, Faculty of Civil Engineering and Architecture, Al. Tysiąclecia Państwa Polskiego 7, 25-314 Kielce, Poland, e-mail: psaternus@tu.kielce.pl, ORCID: 0000-0002-1329-5536

³BEng, MSc, PhD, DSc, Assoc. Prof., Kielce University of Technology and Architecture, Faculty of Civil Engineering, Al. Tysiąclecia Państwa Polskiego 7, 25-314 Kielce, Poland, e-mail: aszychow@tu.kielce.pl, ORCID: 0000-0003-1653-0324

1. Introduction

The dynamic development of visually lightweight architectural forms in metal-glass building envelope structures necessitates the use of increasingly large spans of support structures. The available types of structures for light façades and metal-glass cladding have one thing in common – they are all located on the inner side of the partition [1, 2]. On the external side, there are only pressure elements holding the glass panes. Meeting the load-bearing capacity and stiffness requirements in the plane of principal bending [3], especially for larger spans, requires the use of complex cross sections, generally aluminium sections of considerable height [4]. A solution known to achieve large spans with reduced weight is elements with openwork webs, such as cellular or castellated I-beams and channel beams as well as structural elements welded from tubular bars with rectangular cross-sections, so-called Vierendeel beams [5, 6]. Such a structural system is also referred to as a diagonalless beam or a strutless beam, which has parallel chords (top and bottom) connected to each other by posts in a rigid manner [7–10]. However, the use of classical diagonalless beams in metal-glass building envelopes also amounts to placing them on the inside of the building, which takes up a considerable amount of space.

Patent no. PL229439B1 [11] discloses a novel, fully demountable structural member for a metal-glass building envelopes (Fig. 1), which attempts to solve the above-mentioned problems. The invention is applicable to the construction of metal-glass roofing or walls (curtains).

2. Characteristics of the member

The construction of the member, used as a bendable beam, is shown in Fig. 1. The invention consists of two chords made of rectangular metal tubes spaced apart from each other in the vertical direction via metal sleeves. Bolts are passed through them. The length of the sleeves is adapted to the height of the glazing unit and sealing depth. The longitudinal spacing of the sleeves is densified from the centre of the element towards the supports.

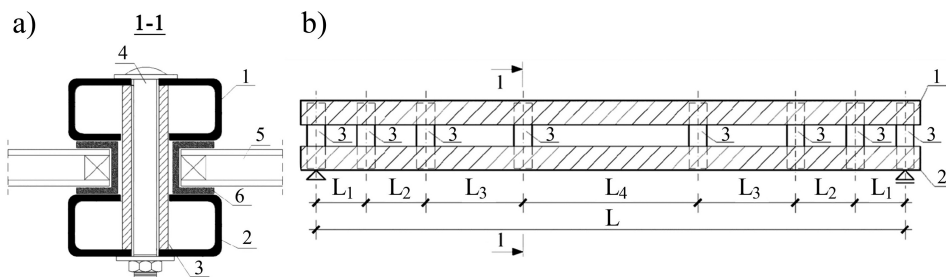


Fig. 1. A two-chord diagonalless beam scheme [11]: a) cross-section, b) side view; 1 – upper chord, 2 – lower chord, 3 – metal sleeve; 4 – bolt, 5 – glass unit, 6 – seal

The chord hole system is designed in such a way that the larger diameter holes located on the inner side of the member allow the sleeves enter the chord space to pass through with a fit. The faces of the cross-section at the ends of the sleeves are then in contact with the inner surface of the outer walls of the chords. In turn, smaller diameter holes in the outer walls of the chords allow the bolts to pass through with a fit. Bolts and sleeves can provide a slip fit and are intended to ensure that the individual parts of the member work together.

In another version of the member, fitting the bolts to the holes is not necessary, and an additional factor to ensure cooperation is the prestress of the bolts. The space between the chords allows the glazing unit to be located in the neutral axis of the bending built-up member, minimising the effect of additional normal stresses transferred from the beam to the seals and glazing [11]. The tangential stresses that occur in this case are compensated for by the deformability of the seals.

This design allows for a relatively high load-bearing capacity and rigidity, as well as a reduction in cost compared to classic solutions made from complex aluminium sections.

3. Main objective of preliminary studies

The solution described in patent no. PL229439B1 [11] is somewhat analogous to the classic Vierendeel beam. The main differences are due to the fact that the chord and post (sleeve) connections do not provide full node stiffness. Their flexibility is influenced by i.a.: 1) the degree of bolt prestress, 2) the accuracy of the fit of components (the chords and sleeves) at their contact surfaces, 3) the flexibility of the chord walls in contact zone with the sleeves. The reduction in nodes stiffness has a direct effect on the distribution of internal forces and on the load-bearing capacity and stability of the member.

The main objective of the first stage of the research is to find out the behaviour under load of a two-chord diagonalless beam of a particular kind and to try to identify possible mechanisms for the exhaustion of its load-bearing capacity. The design of the member is unusual, which raises problems related to the development of computational models that take into account, among other things, contact phenomena, unavoidable clearances in the connections and the degree of fit and prestress of the bolts.

4. Choice of models and programme of the research

For the purposes of the analysis, four static schemes differing in the spacing of sleeves along the length of the beam with a span of $L = 4$ m span were considered, Fig. 2. Schemes M1 and M2 each have seven segments, M3 is a beam like M1 with an additional sleeve in the middle of the span (eight segments) and M4 has eight segments of equal length. Dimensions are given in component bar axes (chords and sleeves).

The research and FEM numerical simulation programme included:

1. Bar model with rigid nodes – the optimum spacing of the posts (sleeves) was determined from the condition of uniform loading by shear forces.

2. Bar model with flexible nodes – the effect of reducing the rotational and translational stiffness of the nodes on internal force distribution and deflection was investigated.
3. Preliminary experimental studies on a trial physical model – a meaningful cognitive effect of the influence of nodes of a unusual design on the behaviour of the member was achieved.
4. Solid model with full wall continuity (1st generation model) – zones of stress concentration, forms of loss of stability were identified and the need for an additional sleeve in the middle of the beam span was revealed.
5. Solid model with incomplete wall continuity taking into account the contact phenomenon (2nd generation model) – a new form of local loss of stability of the chord facewall was observed, i.e. the sliding push effect of the chord wall on the sleeve (within the larger openings) and the phenomenon of changing the distribution and magnitude of the maximum stresses along the length of the member.

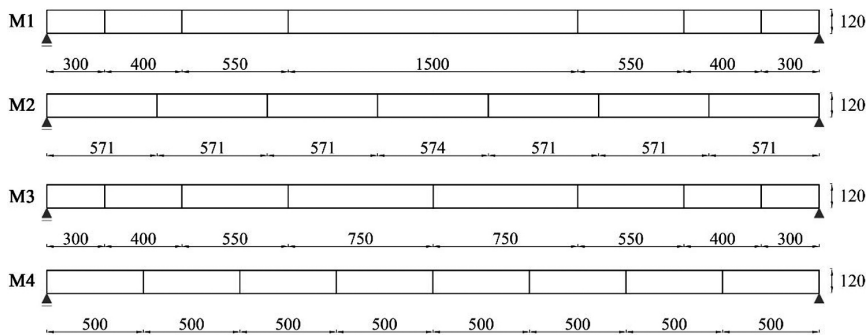


Fig. 2. Considered variants of sleeves arrangement in the member

The research programme focused on identifying the phenomena occurring in the new structural member in order to lay the groundwork for further, more advanced analyses.

5. Bar model with rigid nodes

5.1. The classic vierendeel beam – equal segment lengths

In a classical Vierendeel beam, the key issue is the stiffness of the nodes and the flexural stiffness of the so-called posts (elements perpendicular to the chords). The basic calculation model is a frame with rigid nodes. Diagonalless beams are a $3n$ -hyperstatic system, where 'n' is the number of equal beam segments [12].

One simplified analytical version of the calculation model introduces hinges located at the mid-span of the elements (chords and posts) forming the beam segments – these are the intersection points of the bending moment diagram with the chord and posts elements. However, studies carried out in this area indicate overestimated values of the cross-sectional forces compared to the results from FEM analysis [13]. The transverse load is applied

at the rigid chord-post nodes. The stiffness and geometric invariance of the system in its plane is ensured by preserving the stiffness of the nodes and not, as in the case of a flat diagonal truss, by the geometric topology of the system with pinned nodes (assuming that the structure is protected against lateral loss of stability from the system plane).

The ultimate resistance of the chords and posts is determined from the interaction of the longitudinal force, the bending moment and the transverse force [14]. The moment at the node is half of the design transverse force of the beam at the centre section of the segment under consideration at an arm equal to half the width of that segment. The maximum Vierendeel bending moments and shear forces occur in the outermost segments, decreasing in subsequent segments going towards the centre of the beam span. The values of the bending moments induced by the Vierendeel mechanism are directly influenced by the length of the individual segments. In this case, the failure mechanism consists of local plasticisation of the peri-nodal zones in the top and bottom chords (plastic hinges at the segment corners) due to the interaction of the Vierendeel moments with the global bending moment generating axial forces in the chords [15].

5.2. Optimisation of post spacing

A simply supported structural member of a metal-glass building envelope was considered, consisting of two chords made of RHS 90 × 50 × 4 (rectangular hollow section) spaced 70 mm apart from each other by means of spacer sleeves (cf. Fig. 15a). The sleeves were made of a circular hollow section with a diameter of 38 mm and a wall thickness of 4 mm. For a representative structural system, a total design uniformly distributed load of 4 kN/m was assumed for a 4.0 m long member. Static calculations were carried out using the calculation program Autodesk Robot Structural Analysis 2022 [16].

Typical Vierendeel beam schemes envisage a uniform spacing of posts along the length of the member, resulting in segments of equal length. Work is known to have sought the optimum spacing and number of posts in deep combination trusses, i.e. diagonal – diagonalless, in order to obtain a more uniform distribution of bending moments, important for the resistance of the welded chord-post joints [17]. However, it can be concluded that the shear-optimal segmentation of a fully diagonalless beam is one that provides a quasi-equal shear intensity per segment (Fig. 3). By ensuring equal distribution of the global shear force field, the following segment lengths can be assumed: $L_1 = 7.5\%$, $L_2 = 10\%$, $L_3 = 14\%$, $L_4 = 37\%$ for $L = 100\%$. A similar approach, adapted to different member spans, is also presented in the patent description [11].

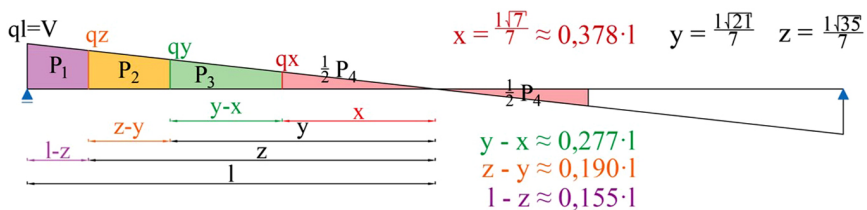


Fig. 3. Method of equal shear force allocation for a beam with 7 segments

However, in order to reduce the buckling length of the compression chord in the middle of the beam span and to ensure its better interaction with the tension chord in flexural-torsional (spatial) forms of beam instability, the above-mentioned lengths of the component segments (determined from the transverse forces condition) were modified by adding a sleeve also in the middle of the member span.

On the basis of the static analysis, it was concluded that the placement of the additional sleeve in the middle of the beam span does not affect the distribution of the normal forces in the chords and has a small effect on the reduction of the Vierendeel bending moments (max. several %), but is important from the point of view of the various forms of loss of stability, as will be demonstrated in the following sections of the article.

6. Bar model with flexible nodes – m3 variant

6.1. Reducing the rotational stiffness of nodes

Simulations of the effect of reducing the degree of rotational stiffness at the member nodes were performed for a bar FEM model in Autodesk Robot Structural Analysis [16]. The dimensionless rotational stiffness ratio varies from $u = 0$ for a pinned node to $u = 1$ for a fully rigid node. The relationship between the dimensionless u -ratio and the dimensional rotational stiffness of the node of the analysed beam can be written according to the formula [18]:

$$(6.1) \quad u = \frac{1}{1 + 3EK/S}$$

where: E – Young's modulus [MPa], $K = I/L_s$ – moment of inertia of the sleeve [m^4] divided by its length in the chord axes [m], S – secant joint stiffness against rotation [kN·m/rad].

6.2. Reducing the translational stiffness of nodes

Due to the peculiarities of the design of the nodes of the diagonalless beam under consideration, slippage may occur at the interface: the end section of the sleeve – the inside of the chord walls.

Simulations of the effect of reducing the degree of translational stiffness of the nodes in the longitudinal direction of the beam were performed for a bar FEM model also in Autodesk Robot Structural Analysis. The dimensionless translational stiffness ratio varies from $v = 0$ for a fully sliding node to $v = 1$ for a fully rigid node per translational displacement.

The relationship between the dimensionless v -ratio and the dimensional translational stiffness of the node of the analysed beam can be written according to the formula:

$$(6.2) \quad v = \frac{S_v L}{EA}$$

where: E – Young's modulus [MPa], L – length of chord segment [m], A – cross-sectional area of the chord [m^2], S_v – secant stiffness of the joint per displacement [kN/m].

6.3. Results of node stiffness analysis

Figure 4 shows the internal forces diagrams (N, V, M) for a representative structural system for $u = 1$ (rigid nodes against rotation), 0.5, 0.1 and $u = 0$ (pinned nodes).

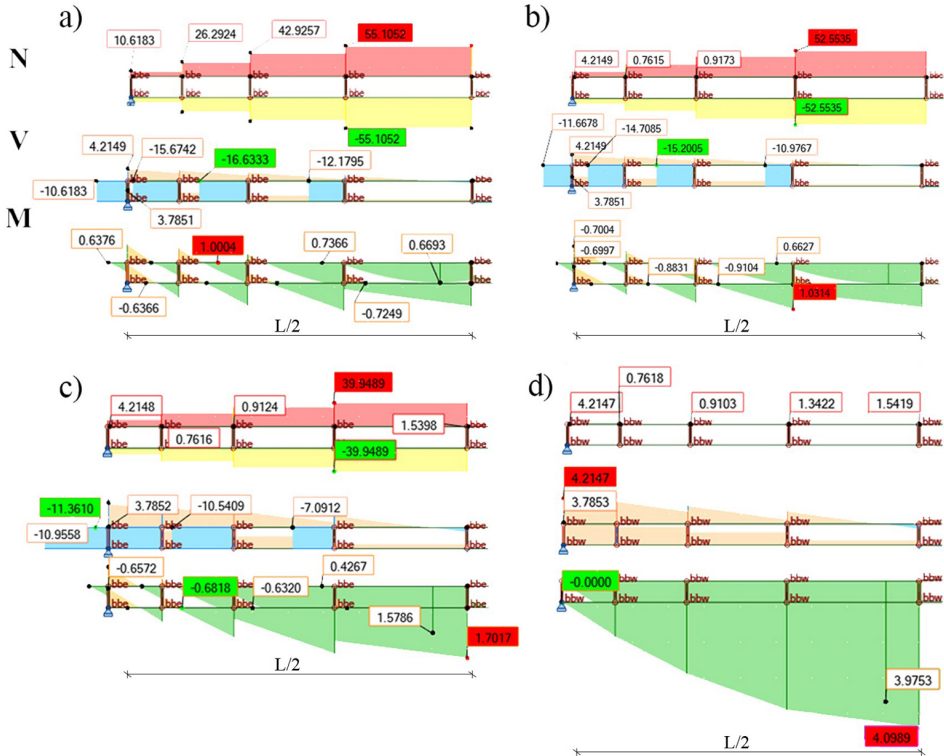


Fig. 4. Diagrams of internal forces (N, V, M) with reduction of rotational stiffness of nodes for: a) $u = 1$, b) $u = 0.5$, c) $u = 0.1$, d) $u = 0$

From a comparison of the diagrams it can be concluded that: 1) as the rotational stiffness ratio decreases, the Vierendeel moments in the chords increase, 2) the largest jump in moment increase occurs between the beam with flexible nodes for $u = 0.1$ and the beam with pinned nodes $u = 0$ (an increase of more than 230%), and the nature and location of the maximum moment also changes, 3) as the value of the u -ratio decreases, the normal forces in the chords decrease. Importantly, the differences in the magnitude of the internal forces between the case of fully rigid nodes and the case of semi-rigid nodes ($u = 0.5$) are negligible. Similar observations have also been obtained by other researchers for Vierendeel beams with equal segment lengths [19], indicating beneficial economic aspects from the use of cheaper semi-rigid nodes in practice.

Figure 5 shows the internal forces diagrams (N, V, M) for a representative structural system for $v = 1$ (rigid nodes against translation), 0.5, 0.1 and $v = 0$ (fully sliding nodes).

The distribution of internal forces when translational stiffness is reduced (Fig. 5) is similar to that shown in Fig. 4. The trend of change remains the same, but the general difference is that for a given value of stiffness ratio, the normal forces are smaller and the shear forces and Vierendeel moments are larger. The type of flexibility at the nodes (rotational or translational) therefore influences the way in which the structural system transfers loads. Longitudinal slippage at the nodes causes shear to play a greater role in the operation of the member under load (increase in shear forces and Vierendeel moments) and the influence of global bending decreases, resulting in lower values of normal forces in the chords.

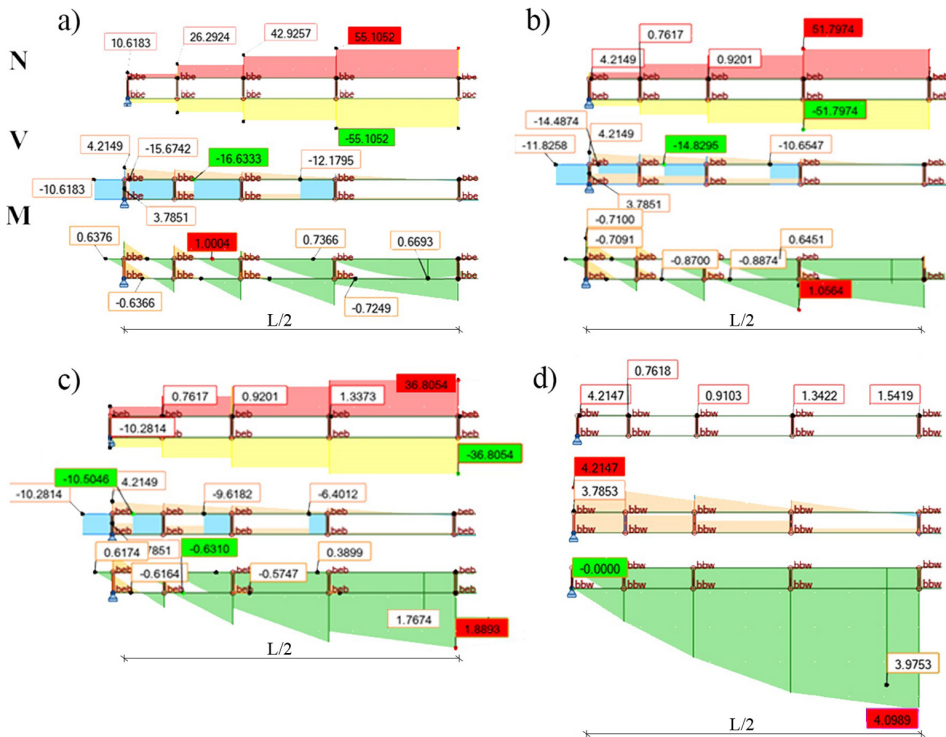


Fig. 5. Diagrams of internal forces (N, V, M) with reduction in translational stiffness of nodes for: a) $\nu = 1$, b) $\nu = 0.5$, c) $\nu = 0.1$, d) $\nu = 0$

Figure 6 shows the dependence of the deflection of the beam at mid-span as a function of the stiffness ratio of the chord-post nodes. The nature of the two curves is strongly similar. In the interval from 1 to 0.3, there is a mildly non-linear reduction (less than 50%) of the beam stiffness as a function of stiffness ratios. The largest increase in deflection was recorded in the interval 0.1 to 0 (an increase of more than 230%). Longitudinal slippage affects the lower capacity to resist global bending and increases the vertical deflection of the element.

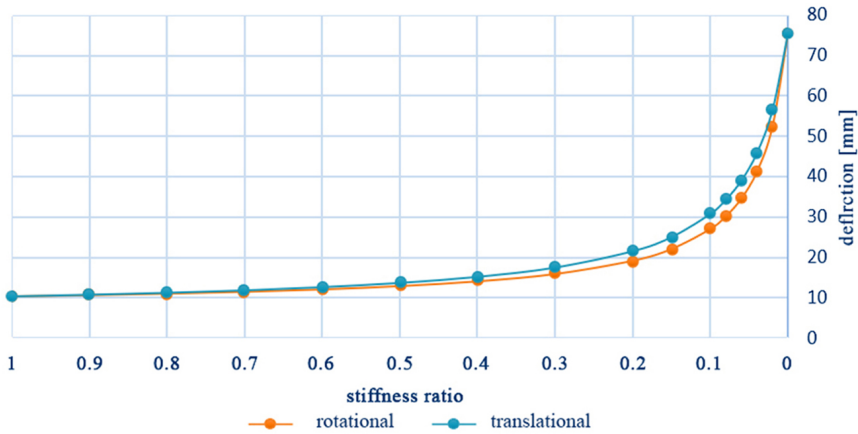


Fig. 6. Dependence of beam deflection as a function of the rotational (u) and translational (v) stiffness ratio

7. Impact of unusual nodes design

7.1. The contact phenomenon

In the two-chord diagonalless member under consideration, the stiffness of the nodes can be ensured by adequate prestress of the bolts in the sleeves and pressure of the sleeves against the edges of the holes in the chord walls. The larger diameter holes (for inserting the sleeves) are located on the inner side of the beam section, while the smaller diameter coaxial holes (for inserting the bolt) are located on the outer side of the chords. As the bolts are prestressed, there will be compression of the end section of the sleeves against the chord walls on the inside. The second component of the internal restraint moment of the sleeve in the chord will be the pressure of the sleeve wall against the edges of the larger diameter holes.

This design of nodes results in contact phenomena in two types of zones. The first contact zone occurs where the sleeve passes through the openings in the lower and upper beam chords – these are the zones of pressure of the sleeve walls against the edges of the holes. The second zone of contact occurs where the end sections of the sleeve come into contact with the flat inner surfaces of the chord walls.

7.2. Preliminary experiment

In order to gain a better understanding of the nature of the static operation of the patented diagonalless member and the influence of unusual nodes design, preliminary experimental tests were carried out. An approx. 1:2 scale model (Fig. 7) in relation to the planned steel test models of natural scale in the M3 variant was used. The sleeves are inserted into the interior of the chords through 20 mm diameter holes, while the M10 cl.10.9 prestressing

bolts (2 washers +1 nut) pass through 12 mm diameter holes (Fig. 7c). The components of the model were made of PA38 aluminium (AW-6060). Material properties: $E = 69500$ MPa, $G = 26100$ MPa, $\nu = 0.33$, density 2.7 g/cm^3 . The structural system of the test model is shown in Fig. 8. The support design (Fig. 7b) approximately fulfilled the theoretical fork support conditions.

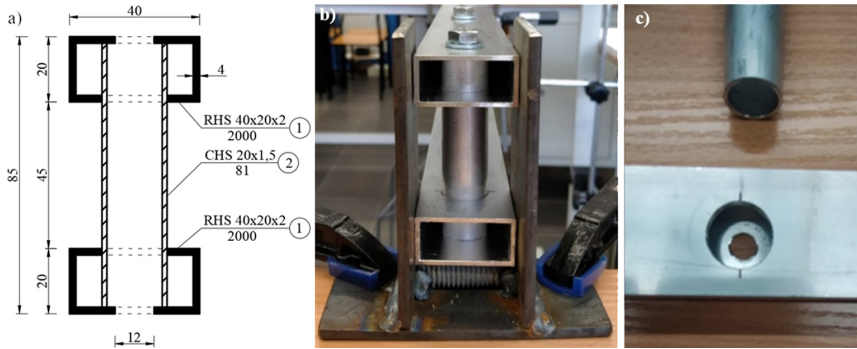


Fig. 7. Preliminary experiment model: a) cross-section through the sleeve, b) view of the beam resting on the support, c) method of chord perforation



Fig. 8. Structural system of the test model

The gravity load, in the form of a force concentrated at the centre of the span, was applied via weights applied to a pan suspended from a protruding bolt shank under the central sleeve. The choice of model material (aluminium) was based on the load application method adopted, which involved allowing free lateral displacements caused by a potential spatial loss of stability and the number of weights available.

Displacement sensors with a measurement accuracy of 0.01 mm were placed in a section located at the point of load application (a vertical beam deflection sensor and lateral displacement sensors for the upper and lower chords). Hand tightening and flat spanner tightening were carried out without strict control of the degree of prestress of the bolts – based on a subjective assessment. Tests were carried out for six variants of bolt tightening:

- Variant 1 – prestressing tighter than to the first spanner resistance; experiment continued to deflection $u = L/200 = 10$ mm; full relief.
- Variant 2 – hand tightening of bolts without a spanner; experiment continued to $u = 10$ mm; full relief,
- Variant 3 – incomplete tightening of bolts, slack; continued to $u = 10$ mm; full relief,

- Variant 4 – prestressing to the first spanner resistance; continued to $u = 20$ mm; full relief,
- Variant 5 – prestressing tighter than to the first spanner resistance; continued to $u = 53.68$ mm; full relief,
- Variant 6 – no correction to bolt prestressing after Variant 5; continued to member failure at $u = 73.38$ mm.

7.3. Results and discussion of the preliminary experiment

Important observations were made during the initial experimental studies, including:

1. The third sleeve from the end of the beam is the boundary point between the small form deformations of the two end segments and the significantly increasing deformations of the longer middle segments (Fig. 9),
2. As the load increased, pressures and clearances zones became apparent at the contact surfaces between the sleeve walls and the edges of the chords holes (Fig. 10) – the phenomenon was most noticeable on the third sleeve from the end of the beam (sleeve no. 3 and no. 7),
3. During the first loading phase, slight values of lateral displacement of the upper and lower chords with opposite directions were observed, indicating torsion of the central section of the beam without a clear lateral displacement of the centre of gravity of the built-up cross-section,
4. During further tests, slight lateral displacements in the middle of the beam span (max. approx. 1 mm) were still recorded at higher load levels, but with the same return for both chords at ratio of approx. 2:1 to the upper chord.

A plot of the static equilibrium path P (load) – w (vertical displacement) for the above-mentioned experimental variants was shown in Fig. 11.

The character of the curves observed in Fig. 11. in the first loading phase indicates that, in the applied loading range, there is a phenomenon of clearance deletion in the zones of potential pressure and a gradual increase in the stiffness of the system (mildly concave character of the $P(w)$ curves). The zones of pressure and clearance revealed were primarily on the edges of larger holes (sleeve sidewall contact with openings on the inside of the built-up cross-section – for each variant). During further loading for Variant 5, a faster completion of the clearance deletion process was observed than in Variant 4, which may be due to a stronger tightening (prestressing) of the bolts. The nature of the path is increasing and convex.

The concavity of the path for Variant 6 probably indicates the influence of the weakening of the micro-strength of the material grains (aluminium) due to the previous plastic deformation from Variant 5. The previous plastic deformations (local indentations) also resulted in clearances and a decrease in prestressing efficiency. The shape of the path indicates a much longer process of clearances deletion and contact zone closure than in Variant 5. Once this process is complete, there is a pronounced flattening of the convex path to fracture of member.



Fig. 9. Deformation of the beam in the plane of principal bending

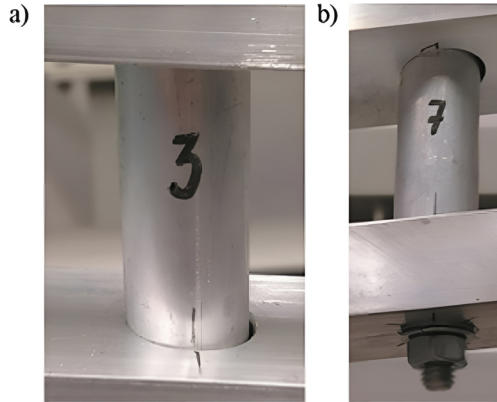


Fig. 10. Sleeves deformation – visible clearances and pressures zones of sleeve – chord hole edges: a) sleeve no. 3, b) sleeve no. 7

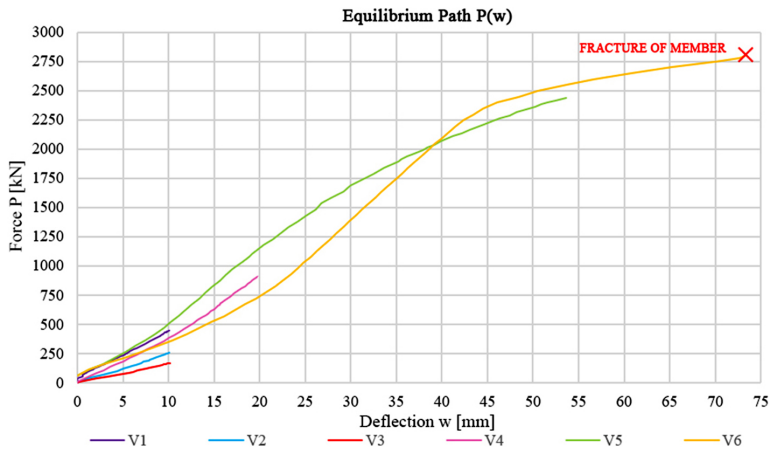


Fig. 11. Equilibrium paths $P(w)$ for the six variants of the experiment

The failure of the model was caused by plasticisation and tearing of the tension chord in the central section weakened by the sleeve and bolt holes, Fig. 12a. The compression flange was partially torn and the upper wall of its section suffered a locally deep indentation under the bolt head, Fig. 12b.

When the built-up member was disassembled, deformations were found in the zones of the smaller holes (contact of bolt/sleeve – outer wall of the built-up cross-section), Fig. 13. Deformations of the sleeves in the contact zones were also noticeable. Pressures of the

chords walls on the sleeves in the plane of the larger holes caused indentations (Fig. 14a), while pressures in the contact zones of the sleeve – outer wall of the built-up cross-section caused deformations in the edge (end) sections of the sleeve, Fig. 14b.

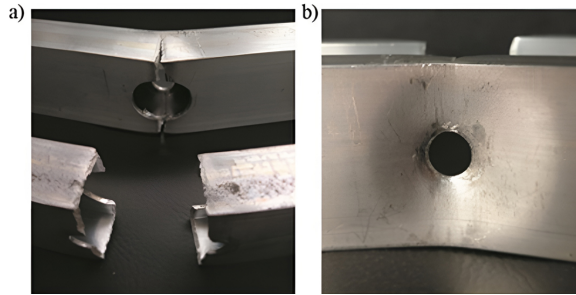


Fig. 12. Failure of the beam: a) section tearing, b) local deformation of the upper chord wall in the middle section

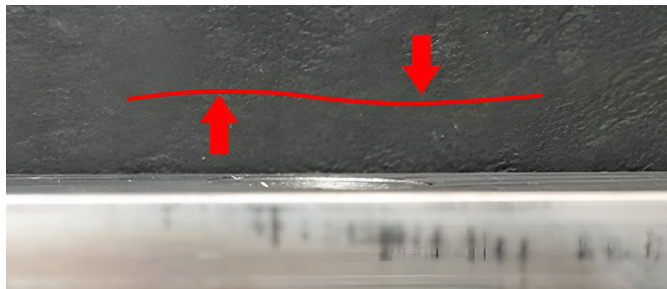


Fig. 13. Deformation of the upper chord around the smaller bolt hole of sleeve no. 3



Fig. 14. Deformations on the sleeves: a) in the pressure zones of the chord walls at the location of the larger holes, b) deformation of the head of sleeve no. 7

Premature tearing of the section at the point of concentrated force action made it impossible to observe local buckling of the chord facewall at larger holes in the sleeve contact zone. In order to investigate this phenomenon, it would be necessary to reinforce the section weakened by holes in the middle of the beam span.

The presence of the central sleeve caused the upper and lower chords to cooperate with each other in terms of torsion and horizontal displacement, so that the phenomenon of

lateral torsional buckling of the beam was not observed. The lateral displacement values recorded, even at higher load levels, indicated a torsion angle of no more than 0.5 degrees.

8. Solid FEM model – rigid nodes vs nodes with contact

8.1. Assumptions for numerical analysis in Abaqus

In order to account for the physical phenomena observed in the preliminary experimental studies (contact, clearances, etc.), spatial (3D) numerical models were built in Abaqus [20] for the beam geometries described in Chapter 4.

The numerical studies compared computational models of two generations:

- 1st generation model – rigid nodes – full walls continuity at each chord-sleeve interface in each segment (“merge” option for the entire model) – used for M1, M2, M3, M4 versions.
- 2nd generation model – partially flexible nodes – lack of material continuity at the interface between the inner walls of the chords and the side surfaces of the sleeve (the phenomenon of contact between the sleeve sidewalls and the edges of the chord walls in the larger holes was taken into account) – used for versions M1 and M3.

The conceptual diagrams of the computational model generations considered was shown in Fig. 15.

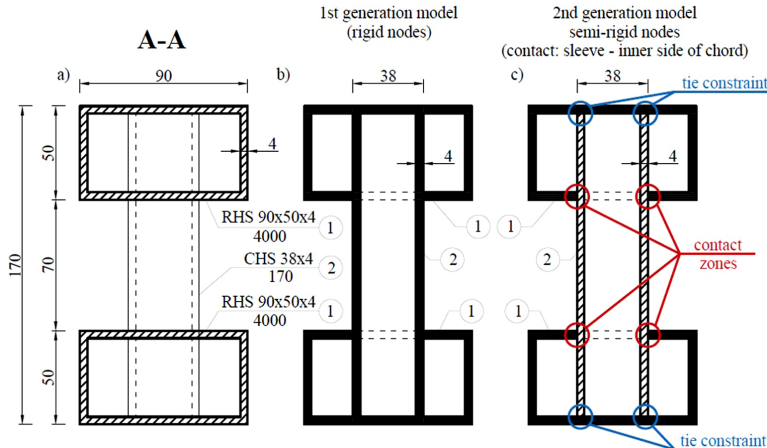


Fig. 15. Geometry and features of two generations of numerical models, a) cross-sectional dimensions, b) 1st generation model, c) 2nd generation model

C3D8R solid elements were used for discretisation. The average mesh size was 10×10 mm with compaction around the sleeve. A material model of steel with linear-elastic characteristics was adopted (Young’s modulus 210000 N/mm^2 , Poisson’s ratio 0.3).

The boundary conditions of the element were modelled to correspond to a simply supported beam. At this stage of the research, the boundary conditions of the supported

sections were applied using so-called reference points. For this purpose, a kinematic coupling (Fig. 16) was used between a reference point located at the centre of gravity of the built-up member support section – at the theoretical axis of the support – and the leading edges of the walls of the component chords. The boundary conditions formulated in this way blocked the vertical displacement of the chords and the longitudinal displacement of the component at the reference point, while not blocking the rotation of the support sections. This way of modelling the support is commonly used, also for built-up members [21, 22]. Consideration of the more complex support conditions of a diagonalless beam, taking into account the structural details of the actual support nodes (the connection of the element under consideration to the rest of the structure) will be the subject of the authors' further research.

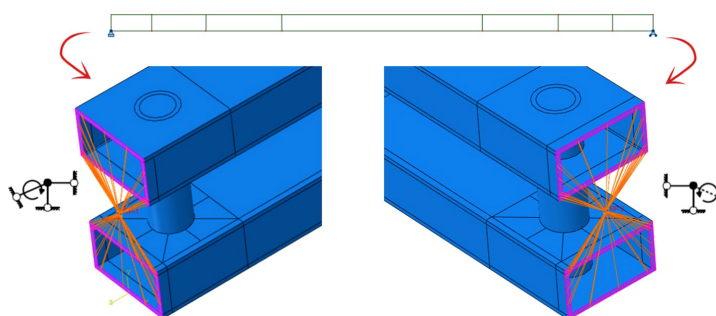


Fig. 16. Boundary conditions at the reference points: a) left side – pinned support, b) right side – roller support (description in text)

A frictionless General Contact was chosen as the method for modelling the contact between the sleeve walls and the chord wall edges in the larger holes (at this stage of the research), and a surface-to-surface contact (Hard Contact) algorithm was used. This numerical model allowed the deformation and stress state of the chord and sleeve walls within their direct contact to be analysed, while assuming 'full continuity' of the material at the chord-sleeve interface within the smaller holes. The analysis of such a model is a starting point and reference point for the next generation of the FEM model, which will be investigated further. The authors believe that this step-by-step approach to solving the task will allow a better assessment of the convergence of the results obtained.

Models were loaded with pressure acting on the top surface of the top chord. In the linear buckling analysis (LBA), a unit load of 0.01 N/mm^2 was applied. In the static analysis (LA), on the other hand, a load of 0.04 N/mm^2 was applied, giving a pre-assumed design linear load of 4 kN/mb of beam.

8.2. Results and discussion of LBA and LA

8.2.1. Stability (LBA)

Table 1 shows the buckling forms associated with the first eigenvalue of these forms of instability for a 1st generation beam without a centre sleeve after segment length optimisation (variant M1) and with a centre sleeve (variant M3). The numerical simulations results obtained confirm the validity of using a sleeve in the middle of the diagonalless beam span.

Note: the eigenvalues shown in Tables 1, 2, 3 and Figs. 17, 18 are multipliers of the unit critical load used in the buckling analysis (i.e. the load applied on the top chord wall, minus the holes, as a surface pressure of 0.01 N/mm²).

Table 1. Buckling forms of the 1st generation model for variants M1 and M3

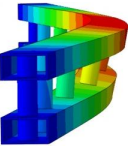
	Beam without middle sleeve	Beam with middle sleeve
First form of loss of stability	 eigenvalue = 85.49	 eigenvalue = 119.45
Buckling in the plane of bending		 eigenvalue = 202.97
Lateral torsional buckling	 eigenvalue = 113.39	 eigenvalue = 190.65

Figure 17 shows the forms of local buckling corresponding to the first (positive) eigenvalue of the loss of stability for the 1st and 2nd generation models.

The buckling analysis showed that for the model with walls discontinuity (2nd generation model), which was replaced by contact zones, a decrease of more than 52% in the eigenvalue of the critical load (from the local buckling condition) was obtained. The nature of the buckling also changed. A new form of local loss of stability of the chord facewall was identified. The lack of wall continuity in the larger holes resulted in sliding push effect of the chord facewalls on the sleeve sidewalls (Fig. 17b). This is a completely different type of chord facewall failure from that found in known tubular welded joints [23, 24].

The critical lateral torsional buckling capacity of the beam also decreased (by more than 27%) compared to the lateral torsional buckling of the 1st generation beam model (Fig. 18). The reason for this decrease is a reduction in the degree of interaction between the compression chord and the tension chord reducing the torsional stiffness of the built-up section.

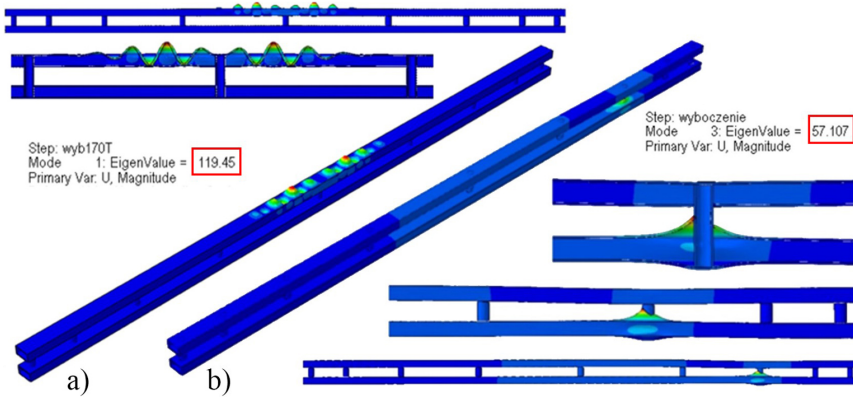


Fig. 17. Forms of instability of chord facewall (local buckling) and critical load multiplier for: a) 1st generation model, b) 2nd generation model

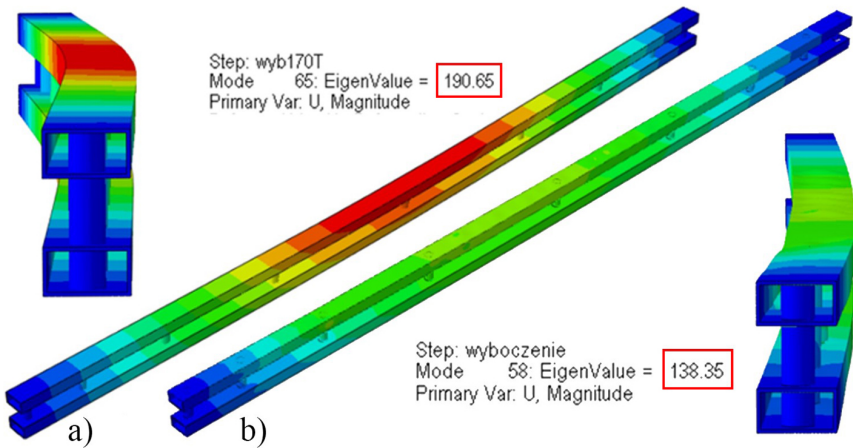


Fig. 18. Global flexural-torsional buckling (lateral torsional buckling) and eigenvalues of the critical load for: a) 1st generation model, b) 2nd generation model

8.2.2. State of stress (LA)

In the diagonalless beam considered in this paper, the cooperation of the chords takes place through the horizontal shear and bending of all the sleeves (except the central sleeve) in the plane of the higher stiffness of the member. The restraint moment of a single sleeve in the chord is generated by the resultant stresses from the pressure zones sleeve against the inner walls of the chords hollow sections and the pressure of the bolts against the smaller holes edges of the chords walls (insufficient prestressing of the bolts) or the frictional forces on the edge (end) sections of the sleeve in contact with inner side of the chord wall (effective prestressing of the bolts).

In the 1st generation model, the concentration of maximum equivalent stresses (Mises stresses) occurred in the cross-section of the third sleeve (counting from the support) in the area between the chords (Fig. 19a). In this case, the maximum principal stresses occurred in the sleeves in the zone of rigid joints with the inner chord walls of the built-up member (full walls continuity of the entire model), Fig. 15c. In contrast, for the 2nd generation model, both the maximum equivalent stresses and maximum principal stresses occurred in the plane of the larger chord holes at the third sleeve (Fig. 19b,d). However, it is worth recognise that the concentration of maximum Mises stresses is at the edges of the chord wall openings, which are the location of the first loss of stability for the 2nd generation model (cf. Fig. 17b). These reached a locally concentrated character with much higher values in contrast to the 1st generation model, where the stresses “spread” over a much larger area.

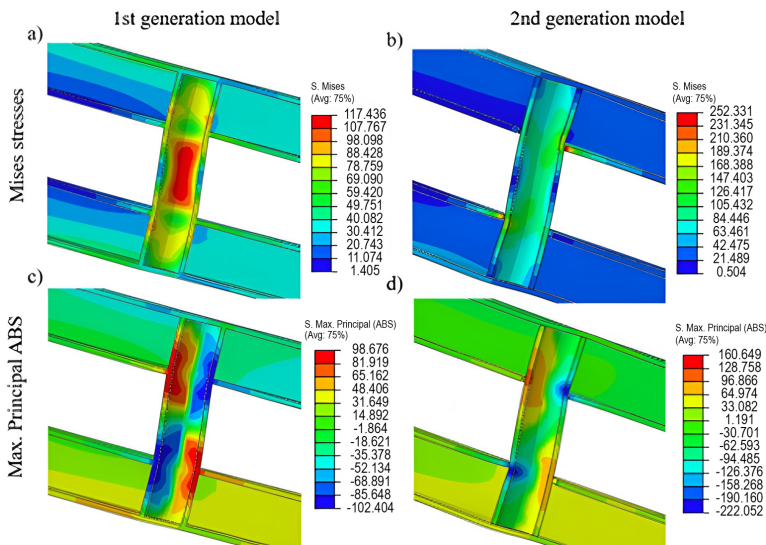


Fig. 19. Location of maximum stresses for 1st generation and 2nd generation model

9. Summary of numerical simulations

Table 2 compares the results of the analysis of the different forms of loss of stability (critical load multipliers), gives the values of equivalent and principal stresses and their location for the two generation models. Importantly, with the partial release of the sleeves in the 2nd generation model, the eigenvalue of local buckling decreased by half with a doubling of the stress in the sleeves.

On the basis of the research carried out, the optimum sleeves spacing for an unusual type of diagonalless beam was determined, taking into account the interaction of shear with global and Vierendeel local bending, as well as the aspects of buckling resistance of the compression chord and the lateral-torsional buckling of the member.

The introduction of the central sleeve was found to give a significant increase in the smallest eigenvalue and a change in the form of buckling (from inter-nodal buckling of the upper chord to local buckling of the chord facewall) – this is a change from a critical load multiplier value of 85.5 (chord buckling) in model M1 to a value of 119.5 (local buckling) in model M3 with the central sleeve, Table 3. The addition of the sleeve in the middle of the span also increases the eigenvalue of the critical load at lateral-torsional buckling. Reduced segment lengths within the mid-span significantly improve the interaction between the upper chord and the lower chord by increasing the torsional stiffness of the section and the eigenvalue at lateral-torsional buckling. On the other hand, the reduced segments lengths near the support zone affects the level of shear stresses in the sleeves and compression stresses within the sleeve – chord wall contact zone (cf. Fig. 19). The lowest stress values were obtained for models M1 and M3, and the highest for model M2. The deflection of the beam for all four variants (M1–M4) remained at the same level. It can therefore be concluded that model M3 is the optimum model due to its high eigenvalues of loss of stability with relatively low equivalent stresses in the sleeves.

Table 2. Statics and stability of 1st and 2nd generation models for variant M3

Model	Stability (Eigenvalue)		Statics			
	Local buckling	Global buckling	σ Mises		Principal stresses	
			Value [MPa]	Location	Value [MPa]	Location
1 st generation	119.45	190.65	117.436	III sleeve, tension	98.676	III sleeve, tension
2 nd generation	57.107 (-52.19%)	138.35 (-27.43%)	252.331 (+114.87%)	Hole at III sleeve, tension	222.052 (+125.03%)	II sleeve, compression

Table 3. Statics and stability of 1st generation models for variants M1–M4

	Eigenvalue			σ Mises		
	Local buckling	Mid-segment buckling	LTB	Sleeve shear [MPa]	Outermost compressed fibres [MPa]	Deflection [mm]
M1	101.52	85.488	113.39	117.375	91.749	9.627
M2	120.50	274.87 (mode: 142)	200.76	138.209	82.108	9.508
M3	119.45	202.97 (mode: 81)	190.65	117.436	80.053	9.213
M4	122.65	309.97 (mode: 160)	204.61	123.730	80.860	9.163

10. Conclusions

On the basis of the numerical simulations and preliminary experimental studies, the following conclusions were drawn:

1. The densification of the segmentation near the support zones is dictated by the law of shear force distribution, while the addition of a sleeve in the middle of the beam span is due to the need to reduce the buckling length of the middle segment with the highest compressive stress level. The introduction of the central sleeve gives a significant increase in the first eigenvalue for variant M3.
2. The lowest shear stresses in the sleeves were obtained for models in M1 and M3 versions with shorter segments near the supports.
3. The stability tests carried out showed a relatively low sensitivity of the member to local buckling, single chord inter-nodal buckling (when a central sleeve is used), and flexural-torsional buckling (lateral torsional buckling). Relatively high critical load multipliers were obtained for these forms of loss of stability.
4. From the stage of research so far, one of the conditions for the design of the beam under consideration is the resistance of the inner chord facewalls (top and bottom) to pressure from the spacer sleeves in the plane of the larger openings (the sliding push effect of the chord facewalls on the sleeve sidewalls – observed in the Abaqus numerical model). The second (inverse) condition relating to the same contact zone is the resistance of the sleeve sidewalls to pressure from the chord facewalls – a phenomenon observed in the experimental study.
5. In planning further experimental studies on life-scale steel models, attention should be paid to the ultimate load capacity of the section of the tension chord weakened by holes (for sleeves and bolts) in the middle of the beam span.
6. The degree of bolt prestress affects the stiffness of the nodes, the distribution of internal forces in the beam components, the magnitude of displacements and the critical load capacity of the various forms of loss of stability.
7. Increasing the flexibility to longitudinal slippage at the nodes, relative to increasing the flexibility to rotation of the nodes in the principal bending plane, results in a lower capacity to resist global bending and increases the vertical deflection of the member. This effect causes an increase in shear forces and Vierendeel moments while reducing normal forces from global bending.
8. The reduction in node stiffness between the case of fully rigid nodes and the case of semi-rigid nodes produces small differences in the magnitudes of the internal forces and deflections.
9. Tests carried out to date confirm the effectiveness of the patented member and show the potential for its use for longer spans. The design of the member allows for easy transport and installation of the glass curtain.

Simulations of the beam's behaviour on 1st and 2nd generation computational models (beam with rigid nodes and beam with partially flexible nodes, respectively) carried out in this study are a necessary introduction to more advanced analyses taking into account contact phenomena, unavoidable and forced clearances and incomplete stiffness in prestressed

nodes. The study of the behaviour of the element for successive generations of the FEM model produced a meaningful cognitive effect of the influence of nodes of a unusual design on the behaviour of the member and allowed, among other things, an assessment of the convergence of the solution.

Further experiments (on life-size steel models) and numerical simulations of the next generation of models (e.g. modelling of bolted connectors, their prestressing and contact phenomenon including friction) will be the subject of future work by the authors.

References

- [1] A. Bojęs and P. Markiewicz, *Przeszkłone ściany osłonowe*. Kraków: Archi-Plus, 2008.
- [2] E. Urbańska-Galewska and D. Kowalski, "Lekka obudowa. Część 4 – układy konstrukcyjne", *Builder*, vol. 233, no. 12, pp. 106–110, 2016.
- [3] E. Urbańska-Galewska and D. Kowalski, "Lekka obudowa. Część 1 – klasyfikacja i wymagania", *Builder*, vol. 227, no. 6, pp. 86–89, 2016.
- [4] D. Kowalski, "The aluminium and polycarbonate covering to the roof over the stadium in Gdańsk", *Steel Construction – Design And Research*, vol. 6, no. 1, pp. 61–66, 2013, doi: [10.1002/stco.201300002](https://doi.org/10.1002/stco.201300002).
- [5] D.J. Wickersheimer, "The Vierendeel", *Journal of the Society of Architectural Historians*, vol. 35, no. 1, pp. 54–60, 1976, doi: [10.2307/988971](https://doi.org/10.2307/988971).
- [6] J.M. Pons-Poblet, "A viga Vierendeel: passado e presente de uma tipologia inovadora", *Arquitectura Revista*, vol. 15, no. 1, pp. 193–211, 2019, doi: [10.4013/arq.2019.151.11](https://doi.org/10.4013/arq.2019.151.11).
- [7] J. Bródka and M. Broniewicz, "Projektowanie belek bezprzekątniowych z kształtowników zamkniętych zgodnie z PN-EN 1993-1", *Inżynieria i Budownictwo*, vol. 65, no. 7, pp. 402–405, 2009.
- [8] J. Bródka and J. Kordjak, "Analiza teoretyczna nośności belek bezprzekątniowych z rur prostokątnych", in *XXXIV Konferencja Naukowa Komitetu Inżynierii Lądowej i Wodnej PAN i Komitetu Nauki PZITB, Gliwice-1988-Krynica*. PAN, 1988, vol. 3, pp. 23–28.
- [9] J. Bródka and J. Kordjak, "Nośność węzłów belek bezprzekątniowych z rur prostokątnych", in *XXXIII Konferencja Naukowa Komitetu Inżynierii Lądowej i Wodnej PAN i Komitetu Nauki PZITB, Gliwice-1987-Krynica*. PAN, 1987, vol. 3, pp. 89–94.
- [10] M. Broniewicz, "Prognozowanie charakterystyki M-fi węzłów belek bezprzekątniowych z rur prostokątnych", *Konstrukcje Stalowe*, no. 6, pp. 41–42, 1999.
- [11] A. Szychowski and P. Obara, "Element konstrukcyjny przegrody metalowo-szklanej", Polish Patent, PL 229439 B1, Jul. 31, 2018.
- [12] S.W. Bryła, "Belki bezprzekątniowe", in *Podręcznik inżynierski*, vol. 1. Warszawa, 1948, pp. 750–756.
- [13] M.K.H. Abdelrahem, "The structural performance of Vierendeel frames using approximate method and computer programs", PhD Thesis, Sudan University of Science and Technology, Sudan, 2018.
- [14] J. Bródka and M. Broniewicz, *Projektowanie konstrukcji stalowych według Eurokodów. Podręcznik inżyniera*. Rzeszów: PWT, 2013.
- [15] M. Grigorian, "A new approach to plastic design and optimization of parallel chord Vierendeel girders", *International Journal of Optimization in Civil Engineering*, vol. 3, no. 3, pp. 371–388, 2013.
- [16] *Autodesk Robot Structural Analysis Professional 2010 Training Manual – Metric Version*. Autodesk Inc., 2009.
- [17] I. Lukačević, M. Ptiček, and D. Dujmović, "Combined lattice and Vierendeel girder in long-span steel frame", *Elektronički Časopis Građevinskog Fakulteta Osijek*, vol. 7, no. 12, pp. 28–38, 2016, doi: [10.13167/2016.12.4](https://doi.org/10.13167/2016.12.4).
- [18] R. Bijak and A. Szychowski, "Długości wybożenia słupów ram w świetle norm", in *56 Konferencja Naukowa KILiW PAN oraz KN PZITB: Problemy Naukowo-Badawcze Budownictwa, 19–24 Sep 2010, Kielce-Krynica*. Kielce, 2010, pp. 141–148.

- [19] A.A. Del Savio, L.F. Martha, S.A.L. De Andrade, P.C.G. da Silva Vellasco, and L.R.O. de Lima, "Structural modelling of Vierendeel beams with semi-rigid joints", in *Proceedings of the XXVI Iberian Latin-American Congress on Computational Methods in Engineering – CILAMCE 2005, Guarapari, Espirito Santo, Brazil, 19–21 Oct 2005*. Brazil, 2005.
- [20] *Abaqus, Theory Manual. Version 6.8*. Hibbit, Karlsson and Sorensen Inc., 2008.
- [21] M. Siedlecka, "Buckling of bipolarly prestressed closely-spaced built-up member", *Archives of Civil Engineering*, vol. 68, no. 3, pp. 23-35, 2022, doi: [10.24425/ace.2022.141871](https://doi.org/10.24425/ace.2022.141871).
- [22] P. Pieczka and P. Iwicki, "Numerical analysis on axial capacity of steel built-up battened columns", *Archives of Civil Engineering*, vol. 68, no. 2, pp. 665-677, 2022, doi: [10.24425/ace.2022.140665](https://doi.org/10.24425/ace.2022.140665).
- [23] M.H. Mussa and A.A. Mutalib, "Effect of geometric parameters (β and τ) on behaviour of cold formed stainless steel tubular X-Joints", *International Journal of Steel Structures*, vol. 18, pp. 821-830, 2018, doi: [10.1007/s13296-018-0031-0](https://doi.org/10.1007/s13296-018-0031-0).
- [24] D.J.R. Pereira, et al., "Effect of chord length on CHS-RHS T-joints with slender sections", *REM-International Engineering Journal*, vol. 74, pp. 433-442, 2021, doi: [10.1590/0370-44672020740135](https://doi.org/10.1590/0370-44672020740135).

Statyka i stateczność belek bezprzekątniowych szczególnego rodzaju – badania wstępne

Słowa kluczowe: belka bezprzekątniowa, dźwigar Vierendeela, dwugałęziowy element złożony, metalowa tuleja, przegrody metalowo-szklane, analiza wyboczenia

Streszczenie:

Atrakcyjne wielkopowierzchniowe przeszklania są obecnie trendem architektonicznym. Jednak osiągnięcie odpowiedniej sztywności przy większych rozpiętościach przeszklania wymaga stosowania skomplikowanych przekrojów poprzecznych, na ogół aluminiowych o znacznej wysokości. W celu uzyskania zwiększonej nośności i sztywności przy zmniejszonej masie stosowane są niekiedy elementy o ażurowych środkach. Wadą takiego rozwiązania jest to, że zabierają one sporo miejsca wewnątrz obiektu. Ostatnio opatentowany bezprzekątniowy element konstrukcyjny stanowi próbę rozwiązania w/w problemów. Element jest w pełni rozbieralny i umożliwia montaż szklanych tafli w przestrzeni pomiędzy pasami. Składa się z dwóch pasów rozsuniętych za pomocą tulei dystansowych, przez które przeprowadzone są śruby. Długość tulei jest dostosowana do wysokości pakietu szyb wraz z uszczelnieniem. Wzdłużny rozstaw tulei zagęszcza się od środka elementu w kierunku podpór. System otworowania pasów wykonany jest w taki sposób, aby otwory o większej średnicy usytuowane od strony wewnętrznej elementu umożliwiały pasowne przeprowadzenie przekroju tulei, które wchodzi do przestrzeni pasów. Powierzchnie czołowe przekroju na końcach tulei stykają się wówczas z powierzchnią wewnętrzną zewnętrznych ścianek pasów. Otwory o mniejszej średnicy w zewnętrznych ściankach pasów umożliwiają z kolei pasowne przeprowadzenie śrub. Śruby z tulejami mogą stanowić suwliwie skojarzenie i mają zapewnić współpracę poszczególnych części elementu złożonego. W innej wersji elementu, pasowanie śrub do otworów nie jest konieczne, a dodatkowym czynnikiem zapewniającym współpracę jest sprężenie śrub. Przestrzeń między pasami umożliwia umieszczenie pakietu szyb zespolonych w osi obojętnej złożonego elementu zginanego, co minimalizuje wpływ dodatkowych naprężeń normalnych przekazywanych z belki na uszczelki i szyby. Natomiast powstające w tym przypadku naprężenia styczne są kompensowane odkształcalnością uszczelek.

Rozwiązanie opisane w patencie nr PL229439B1 jest w pewnym stopniu analogiczne do klasycznej belki Vierendeela. Zasadnicze różnice wynikają stąd, że połączenia pasów i słupków (tulei) nie zapewniają pełnej sztywności węzłów. Na ich podatność wpływają m.in.: 1) stopień sprężenia śrub,

2) dokładność dopasowania elementów składowych (pasów i tulei) na powierzchniach ich styku, 3) podatność ścianek pasów w obszarze kontaktu z tulejami. Do celów analizy rozważono cztery schematy statyczne różniące się rozmieszczeniem tulei dystansowych na długości belki. Program badań i symulacji numerycznych obejmował:

1. Model prętowy o sztywnych węzłach – wyznaczono optymalny rozstaw słupków (tulei) z warunku równomiernego obciążenia siłami tnącymi.
2. Model prętowy o węzłach podatnych – zbadano wpływ redukcji sztywności obrotowej i translacyjnej węzłów na rozkład sił wewnętrznych i ugięcie.
3. Wstępne badania doświadczalne na próbnym modelu fizycznym – osiągnięto wymierny efekt poznawczy wpływu węzłów o szczególnej konstrukcji na zachowanie się elementu, a także rozpoznano strefy wrażliwe na lokalne deformacje, m.in. strefa kontaktu ścianek bocznych tulei z krawędziami większych otworów w ściankach pasa.
4. Model bryłowy o pełnej ciągłości ścianek (model 1. generacji) – zidentyfikowano strefy koncentracji naprężeń, formy utraty stateczności oraz ujawniono potrzebę wprowadzenia dodatkowej tulei w środku rozpiętości belki.
5. Model bryłowy o niepełnej ciągłości ścianek przy uwzględnieniu zjawiska kontaktu (model 2. generacji) – zaobserwowano nową formę lokalnej utraty stateczności pasa, tzw. efekt przesuwnego napierania ścianki pasa na tuleję (w obrębie otworów większych). Jest to zupełnie inny rodzaj uszkodzenia ścianki czołowej pasa niż ten, który występuje w znanych rurowych połączeniach spawanych. Wystąpiły również zmiany dystrybucji i wielkości maksymalnych naprężeń na długości elementu.

W artykule wykazano, że zagęszczenie podziału na segmenty przy podporach jest poddyktowane prawem rozkładu sił tnących, natomiast dodanie tulei w środku rozpiętości belki wynika z potrzeby zmniejszenia długości wybojcowej środkowego segmentu z największym poziomem naprężeń ściskających. Wprowadzenie środkowej tulei daje znaczący wzrost pierwszej wartości własnej. Krótsze segmenty przy podporach skutkują niższymi naprężeniami ścinającymi w tulejach. Zwiększanie podatności na poślizg podłużny w węzłach, w stosunku do zwiększania podatności na obrót węzłów w płaszczyźnie głównego zginania, powoduje mniejszą zdolność przeciwstawiania się zginaniu globalnemu i zwiększa pionowe ugięcie elementu. Efekt ten wywołuje wzrost sił tnących i momentów Vierendeela przy jednoczesnej redukcji sił normalnych od zginania globalnego. Redukcja sztywności węzłów między przypadkiem węzłów w pełni sztywnych a przypadkiem węzłów półsztywnych wywołuje niewielkie różnice w wielkościach sił przekrojowych i ugięciach.

Program badań koncentrowała się na identyfikacji zjawisk zachodzących w nowym elemencie konstrukcyjnym w celu stworzenia podstaw do dalszych, bardziej zaawansowanych analiz. Dalsze badania doświadczalne (na modelach stalowych w skali naturalnej) i symulacje numeryczne kolejnych generacji modeli (m.in. modelowanie łączników śrubowych, ich sprzężenia i stref kontaktu z uwzględnieniem tarcia) będzie przedmiotem kolejnych prac autorów.